Scientific Reports

https://doi.org/10.1038/s41598-026-44930-6

Article in Press

A novel arc signal and motor power synchronization-based method for precise contact fault diagnosis of GIS disconnector

Received: 3 January 2025

Accepted: 16 March 2026

Published online: 02 April 2026

Cite this article as: He S., Ruan J., Liu Y. *et al.* A novel arc signal and motor power synchronization-based method for precise contact fault diagnosis of GIS disconnector. *Sci Rep* (2026). https://doi.org/10.1038/s41598-026-44930-6

Song He, Jiangjun Ruan, Yufei Liu, Feiyue Yan & Rui Luo

A Novel Arc Signal and Motor Power Synchronization-Based Method for Precise Contact Fault Diagnosis of GIS Disconnector

Song He[1], Jiangjun Ruan[1,*], Yufei Liu[1], Feiyue Yan[1], Rui Luo[2]

[1] Hubei Key Laboratory of Power Equipment & System Security for Integrated Energy, School of Electrical Engineering and Automation, Wuhan University, Wuhan 430000, Hubei Province, China

[2] Wuhan Hongmen Electrical Technology Co., Ltd., Gezhouba Sun City Building 16, Wuhan 430000, Hubei Province, China

[*]**Corresponding author: Jiangjun Ruan, Email: ruan308@126.com**

Abstract

Gas-insulated switchgear (GIS) disconnectors play an important role in power systems, and their mechanical condition is critical for operational reliability. However, existing diagnostic methods frequently fail to accurately identify critical operational states during switching processes, such as the initial contact and separation points. This study proposes a novel diagnostic approach that combines arc signal detection and motor power analysis to address these limitations. The arc signal captured by a Rogowski coil provides precise timing information for contact engagement and separation. An adaptive wavelet packet decomposition method, guided by power spectral entropy, is used to effectively denoise the arc signal, allowing for precise extraction of ignition and extinction points. By synchronising the arc signal with motor power data, the proposed method makes it easier to diagnose common mechanical faults such as refusal to close, refusal to open, insufficient overtravel, and insufficient opening distance. Experimental validation confirms the method's robustness and reliability, emphasising its potential for improving GIS disconnector fault diagnosis and system reliability.

Keywords: GIS disconnector diagnostics; arc signal analysis; motor power synchronisation; mechanical fault detection; adaptive layering process

1. Introduction

Gas-insulated switchgear (GIS) disconnectors are critical components of modern power systems, ensuring the grid's safety and reliability [1]. The mechanical condition of these disconnectors directly impacts the power system's performance and stability [2-4]. Faults such as refusal to close or open, insufficient closing stroke, and insufficient opening distance can cause increased contact resistance, overheating, ground discharge, and ultimately system failure [5, 6]. The enclosed structure of GIS disconnectors makes direct observation of the contact state between moving and static contacts nearly impossible. This limitation necessitates the development of non-invasive diagnostic techniques to monitor the mechanical state of disconnectors and ensure their proper operation.

Existing studies have explored several approaches for diagnosing the mechanical state of GIS disconnectors, including analysing motor power curves [7], vibration signals [8-10], and operation torque signals [11] during switching operations. Scholars have used techniques like support vector machines (SVM) [12], genetic algorithms (GA) with density-based clustering [13], and convolutional neural networks (CNN) with evidence theory [14]. While these methods provide valuable insights into operational behaviour, they do not accurately identify critical switching

points like the initial separation and contact points. These points are critical for determining the correct operation of the disconnector and evaluating parameters such as stroke distance and overtravel. In addition, it should be noted that most existing diagnostic approaches for GIS disconnectors are predominantly data-driven. These methods mainly rely on statistical features extracted from motor power, vibration, or torque signals, and their diagnostic performance depends heavily on signal patterns and learning algorithms, while lacking explicit physical criteria directly associated with contact engagement and separation processes.

In contrast, the proposed method is fundamentally physics-driven. It exploits the inherent physical mechanism of arc generation during contact approach and separation, where arc ignition and extinction correspond to well-defined electrical and mechanical states of the disconnector. By using arc signals as physically interpretable indicators and synchronising them with motor power, the proposed approach provides clear and reliable criteria for identifying critical switching points, thereby enhancing interpretability and robustness compared with conventional data-driven methods.

An important challenge in arc signal detection is the interference caused by environmental noise and power ripple in the detection circuit. Given the complexity and chaos of these signals, traditional filtering techniques frequently fail to effectively denoise them. This study introduces an adaptive wavelet packet decomposition method based on power spectral entropy to address this issue. The proposed approach

improves the accuracy of ignition and extinction point detection by effectively removing noise while retaining critical features.

Experiments and engineering practices have confirmed the method's efficacy, demonstrating its potential to improve fault diagnosis for GIS disconnectors. This study provides a strong and innovative approach to ensuring the reliable operation of GIS equipment and advancing non-invasive diagnostic techniques for power systems.

2. Physical Process and Diagnostic Implications

2.1. Physical Process and Cause of Arc Signal Generation

The arc signal in a GIS disconnector is caused by an electrical discharge between the moving and static contacts during switching operations. When the GIS disconnector is activated, an arc discharge occurs when the gap between the contacts becomes sufficiently tiny, resulting in a high-intensity electric field that ionises the surrounding insulating medium, such as air or a specialised gas. This phenomenon differs during the closing and opening processes.

During the closing process, the moving contact begins at a significant distance from the static contact, where no arc discharge occurs. As the contacts get closer, the gap narrows to a critical point where an arc discharge occurs. The arc continues until the contacts physically touch, resulting in a conductive metal path. The moment of arc extinction corresponds to the first contact point, after which the moving contact travels a short distance, known as overtravel. This overtravel is critical for ensuring an adequate metal contact area and reducing contact resistance.

Insufficient overtravel can result in high contact resistance, which can cause thermal faults and pose operational risks.

The moving and static contacts maintain solid metal connections without arc discharge during the opening process. When the moving contact begins to separate, and the gap reaches a critical size, an arc discharge is initiated. The arc continues until the contacts are sufficiently separated, at which point it dissipates. The cessation of the arc indicates establishing a safe separation distance, which ensures adequate electrical isolation.

The arc signal, detected by a Rogowski coil, appears as high-frequency pulses that capture the exact moment of arc initiation and extinction. These signals reflect the contacts' dynamic behaviour during switching and provide important diagnostic information. When combined with other diagnostic signals, such as motor power, the arc signal improves the accuracy of determining contact state, allowing for precise fault diagnosis and operational assessments.

2.2. Diagnostic Implications of Arc Signal and Motor Power Signal Synchronization

As shown in Fig. 1, synchronising the arc signal with the motor power signal provides several diagnostic insights for assessing GIS disconnectors' mechanical state.

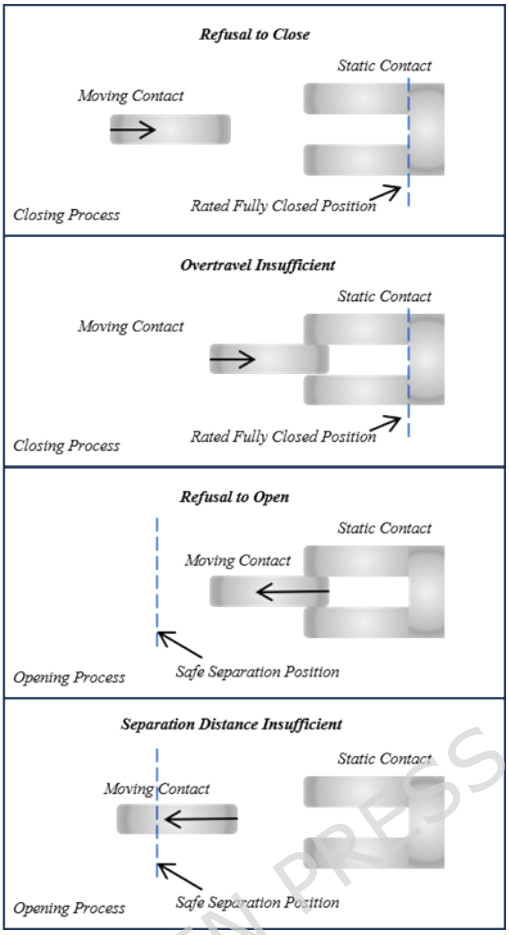

Fig. 1. Fault mechanical state of GIS disconnectors.

1) Refusal to close fault diagnosis:

The presence or absence of an ignition point in the closing arc signal indicates whether a refusal to close fault has occurred. The moving contact does not reach the critical discharge distance if no ignition is detected. The motor power signal further supports this diagnosis, which indicates whether the contact movement was completed.

2) Initial contact and overtravel determination:

The closing arc signal's extinguishment point corresponds to the motor power signal's initial contact. This moment is a criterion for determining whether the contacts have adequately engaged. Furthermore, the time

between arc extinguishment and the end of the motor power signal is known as the overtravel period, which is critical for ensuring adequate metal contact and avoiding excessive contact resistance.

3) Refusal to open fault diagnosis:

In the opening process, the presence or absence of an ignition point in the arc signal indicates whether a refusal to open fault occurred. A lack of ignition indicates that the moving contact did not separate sufficiently to cause discharge. The motor power signal supports this conclusion and provides additional confirmation.

4) Safe separation distance diagnosis:

The extinguishment point of the opening arc signal corresponds to setting a safe separation distance in the motor power signal. This value is used as a diagnostic criterion to determine whether the GIS disconnector provides adequate separation for proper electrical isolation.

Faults such as refusal to close or open, insufficient overtravel, and insufficient separation distance can be diagnosed more precisely using this synchronised arc and motor power signal analysis. This integrated approach improves the reliability of mechanical state assessments in GIS disconnectors, ensuring operational stability and mitigating maintenance risks.

3. Math

After determining the diagnostic significance of the arc signal in detecting mechanical faults in GIS disconnectors, the next step is to process the signal to ensure accurate fault detection. The arc signal is

captured by a Rogowski coil, which detects the transient current produced during the arc burning process. This signal is then sampled using an oscilloscope or an AD (analogue-to-digital) sampling device for further analysis. However, the raw arc signal contains significant noise, which can be caused by environmental white noise or power supply ripple in the detection circuitry. These noise components can obscure important diagnostic features of the arc signal, such as the ignition and extinguishment points, making detection difficult. Therefore, an effective denoising technique is required.

3.1. Wavelet Packet Denoising

Wavelet packet decomposition (WPD) reduces noise in the arc signal [15-17]. Unlike traditional wavelet transforms, WPD decomposes the approximation and detail coefficients, allowing for finer analysis across multiple frequency bands. This feature is handy for the arc signal, which contains high-frequency noise and low-frequency components.

The mathematical expression for the wavelet packet decomposition of a signal f(t) at level j is:

$$f_j(t) = \sum_k c_{j,k} W_{j,k}(t) \quad (1)$$

where j represents the decomposition level (or layer), k indicates the position index corresponding to different frequency sub-bands at each level, $W_{j,k}(t)$ are the wavelet packet basis functions, and $c_{j,k}$ are the wavelet packet coefficients at level j and position k.

This study used the Symlet 6 wavelet for signal decomposition and denoising. Symlet 6 is a Symlet family member, designed to be symmetric with minimal vanishing moments, making it ideal for signal processing

tasks. The wavelet is defined by a specific analytical expression derived from its scaling and wavelet functions, designed to meet certain smoothness and symmetry requirements. This wavelet ensures effective signal separation and noise reduction while retaining the inherent characteristics of the original signal.

3.2. Adaptive Layering Based on Power Spectral Entropy

An adaptive method based on power spectral entropy is introduced to ensure the wavelet packet decomposition is applied to the maximum depth. Power spectral entropy assesses the signal's energy distribution complexity across frequency components. Higher entropy indicates a more complex or noisy signal, whereas lower entropy indicates a structured signal with fewer dominant frequencies.

The power spectral entropy E is defined as [18, 19]:

$$E = -\sum_i P_i \log(P_i) \tag{2}$$

where P_i represents the normalized power in the ith frequency band.

The adaptive layering process involves the following steps:

Initial entropy calculation: Compute the power spectral entropy E_{orig} of the original arc signal.

Wavelet packet decomposition: Decompose the signal into multiple levels using wavelet packets. After each decomposition level, reconstruct the signal and compute its power spectral entropy E_j at level j.

Entropy comparison: Compare the reconstructed signal's entropy E_j to the original entropy E_{orig}. The decomposition process stops when the entropy decreases by a predefined ratio α. This adaptive approach ensures that the wavelet packet decomposition is used only when necessary,

preventing overprocessing while preserving critical signal features.

Algorithm 1 expresses the process as follows:

Algorithm 1

$E_{\text{orig}} \leftarrow \text{PowerSpectralEntropy}(X)$

$j_{\text{opt}} \leftarrow 1$

$W_1 \leftarrow \text{WaveletPacketDecompose}(X,1)$

$for\ j\ =\ 2\ \ to\ J_{max}$:

$\widetilde{X}_j \leftarrow \text{WaveletPacketReconstruct}\left(W_{j-1}\right)$

$E_j \leftarrow \text{PowerSpectralEntropy}\left(\widetilde{X}_j\right)$

$\text{if}\ E_j \leq \alpha E_{\text{orig}}$

$j_{\text{opt}} \leftarrow j-1$

break

else

$W_j \leftarrow \text{WaveletPacketDecompose}\left(\widetilde{X}_j, j\right)$

$\hat{X} \leftarrow \text{WaveletPacketReconstruct}\left(W_{j_{\text{opt}}}\right)$

4. Experimental Setup and Procedure

Fig. 2 shows the experimental setup for testing the GIS disconnector, while Fig. 3 shows the experimental site scenario. The system is designed to accurately monitor and diagnose the mechanical and electrical characteristics of the ZF12B-126 GIS disconnector, integrating several key components. A Rogowski coil captures transient current signals generated during the arc process, focusing on high-frequency components monitored using an oscilloscope. To maintain controlled operational conditions, the

GIS disconnector is linked to a transformer and water resistance units, which regulate and stabilise the voltage and current levels in the test circuit.

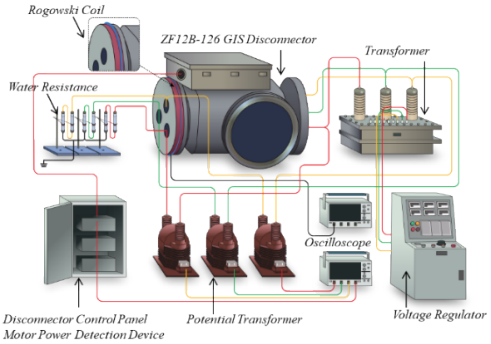

Fig. 2. A schematic diagram of the experimental setup for testing the ZF12B-126 GIS disconnector.

Fig. 3. Experimental site scenario.

A potential transformer monitors voltage and a voltage regulator adjusts and maintains the required voltage levels throughout the experiment. The disconnector control panel allows for precise operation of the disconnector, and the device for detecting motor power records motor power signals. Together, these components provide critical data for evaluating the disconnector's performance during opening and closing operations, ensuring that the mechanical and electrical behaviours are thoroughly analysed.

Table 1 summarises the basic parameters of the equipment involved to provide a clear understanding of the key components and their specifications for the experimental platform. These parameters are critical for ensuring accurate data acquisition and analysis during the testing of the GIS disconnector, which affects the reliability and precision of the experimental results.

Table 1 Basic parameters of experimental platform components

Component	Parameter	Value
Rogowski Coil	Sensitivity	50 mV/kA
Transformer	Rated Voltage	50 kV
Water Resistance	Resistance Value	2.5 MΩ
Potential Transformer	Voltage Accuracy	±0.5%
Oscilloscope	Memory Depth	10 Mpts
Power Detection Device	Sample Frequency	1 kHz

The motor power was measured at a sampling rate of 1 kHz to capture the motor's voltage and current signals. The average power method was used to determine the motor's power. The instantaneous voltage and current signals were sampled simultaneously at 1 kHz, and the instantaneous power was calculated as the product of these signals. The motor power was then calculated by averaging the instantaneous power over a predetermined time interval, accurately representing the motor's

operational power under varying loads. The procedure can be expressed as:

$$P_{\text{avg}} = \frac{1}{N}\sum_{n=1}^{N} P(n) = \frac{1}{N}\sum_{n=1}^{N} V(n) \times I(n) \quad (3)$$

where P_{avg} is the average power, N is the total number of sampling points in a single period (in this case, N = 20), $P(n)$ is the instantaneous power at the n^{th} sample, and $V(n)$ and $I(n)$ are the voltage and current at the n^{th} sample, respectively.

During motor power detection, the oscilloscope uses a voltage-feedback-type current transformer to detect the motor's current signal while simultaneously sampling the motor's voltage and current. Once the data is collected, the oscilloscope's arc signal data and the data for detecting motor power are synchronised based on the current signal. This synchronisation ensures a unified reference time across all signals, allowing accurate data alignment and subsequent analysis.

5. Experimental Results and Analysis

5.1. Synchronized Analysis of Arc Signal and Motor Power

Fig. 4 illustrates the power profile of the drive motor (top) and the discharge signal (bottom) during the GIS disconnector's opening process; the two signals are time-synchronised for precise analysis.

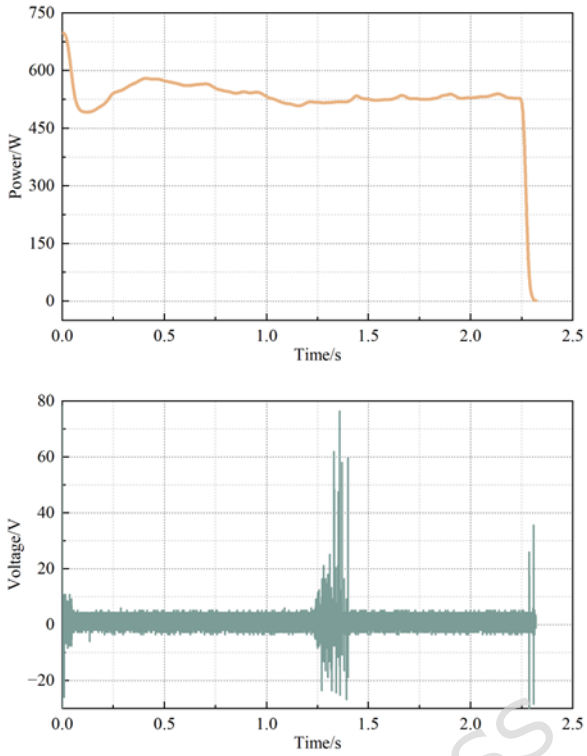

Fig. 4. The drive motor (top) and the corresponding discharge signal (bottom) during the opening process.

In the investigated disconnector, the drive motor operates under open-loop control, and the motor power endpoint is clearly identified by the rapid drop of measured motor power to near zero within one power cycle after the limit switch cuts off the motor supply.

During contact separation, the motor power increases significantly as the contacts pull apart, reflecting the additional energy required. At about 1.25 seconds, the contacts reach the critical separation point, the initial separation point. The onset of the discharge signal indicates that an arc discharge is currently taking place. As the gap between the moving and static contacts widens, the breakdown voltage rises, resulting in higher peak discharge signal values. This trend correlates with contact separation distance and arc intensity during the opening process.

The Rogowski coil detects the arc signal, representing the capacitance's charging and discharging current formed between the static contact and the GIS enclosure. As the gap widens, the breakdown voltage increases, raising the capacitance's charging voltage. Because the capacitance remains constant, the increase in voltage directly results in increased charging and discharging current. This increase is reflected in the arc signal as rising peaks, demonstrating the effect of contact separation on both the breakdown voltage and the capacitance current.

This relationship in the opening process has a symmetrical counterpart in the closing process (Fig. 5). As the moving contact approaches the static contact, the gap narrows, lowering the breakdown and charging voltages of the capacitance. This voltage reduction causes a corresponding decrease in charging and discharging current. The arc discharge weakens and eventually dissipates at the initial contact point, indicating the formation of a metallic conductive pathway. After this point, the contacts are fully engaged, and the charging and discharging currents decrease further. This trend is reflected in the arc signal, which gradually decreases in peak values until it disappears entirely. This process effectively captures contact engagement behaviour and demonstrates how the arc signal is an important diagnostic tool for determining the mechanical state of GIS disconnectors.

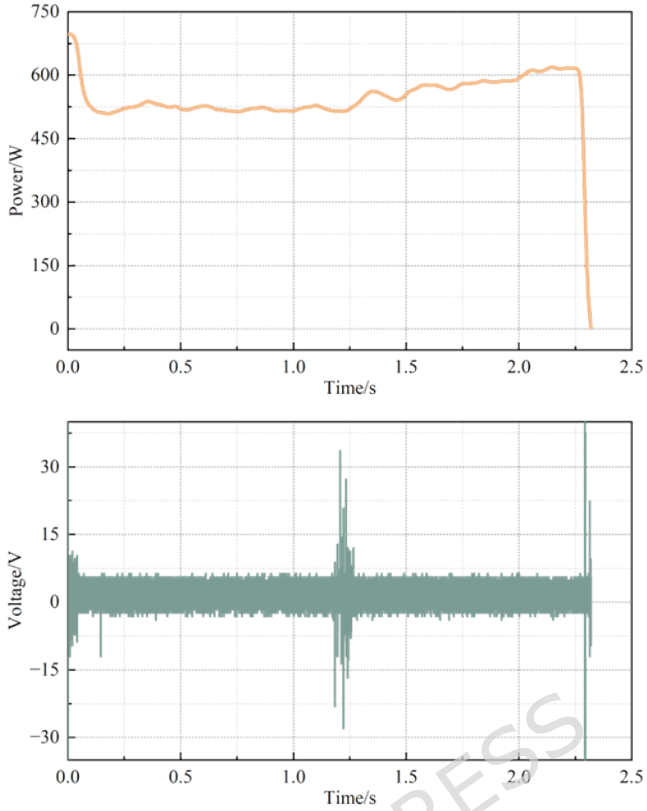

Fig. 5. The drive motor (top) and the corresponding discharge signal (bottom) during the closing process.

5.2. Arc Signal Denoising Based on Adaptive Wavelet Packet Decomposition

A denoising process based on adaptive wavelet packet decomposition was used to improve the diagnostic potential of arc signals and ensure the accuracy of ignition and extinction point identification.

Fig. 6 compares the arc signal before and after denoising with the proposed adaptive wavelet packet decomposition method. The original signal (top) has significant noise throughout the recording, obscuring the arc signal's key features, such as its peak values and temporal evolution. This noise makes it difficult to accurately identify critical points like the arc's ignition and extinction.

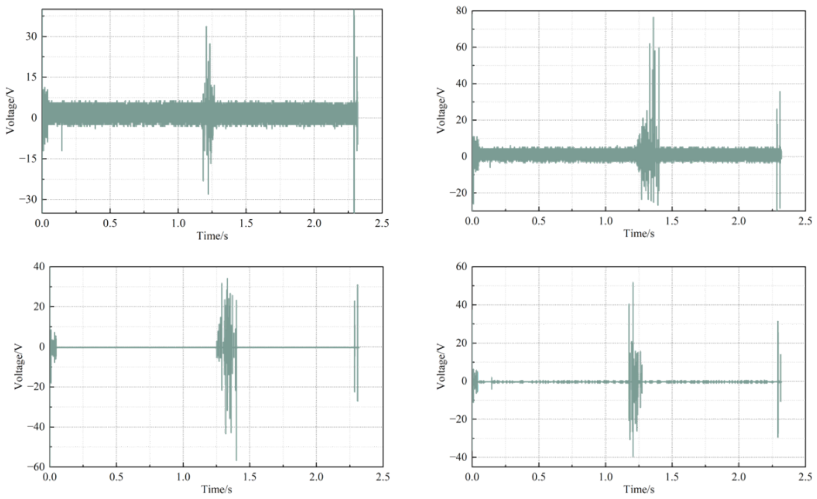

Fig. 6. Comparison of the arc signal before (top) and after (bottom) denoising.

The arc signal's structure is much clearer after denoising with the adaptive wavelet packet method (bottom). The noise components have been effectively suppressed, making it easier to determine the start and end points of the arc signal. This improvement allows for precise time alignment and further analysis.

This comparison demonstrates how effective the proposed denoising method is at preserving the arc signal's essential features while eliminating interference, making it more usable for subsequent analysis.

5.3. Power Spectral Entropy Analysis and Denoising Performance Evaluation

The entropy analysis of arc signals was carried out using the previously described experimental setup, with 367 samples collected over three consecutive days. The upper portion of Fig. 7 shows the initial entropy values of the arc signals. In contrast, the lower portion shows the entropy values after achieving the desired denoising effect using the adaptive

wavelet packet decomposition technique. The results show that using a power spectral entropy threshold effectively stops wavelet packet decomposition at the optimal level, ensuring that the denoising goal is met without requiring additional decomposition.

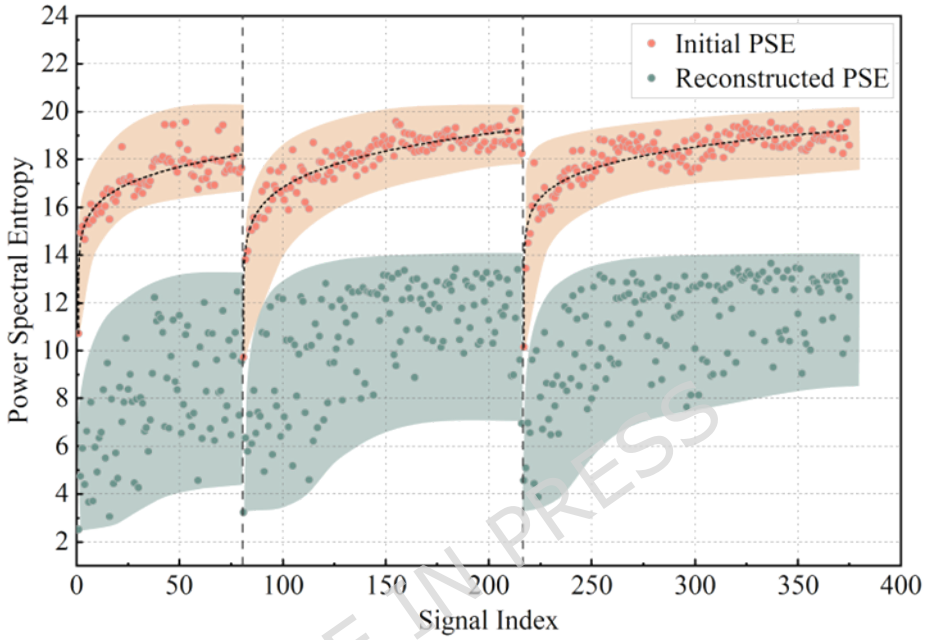

Fig. 7. Entropy analysis of the arc signals.

Fig. 8 illustrates the variation of power spectral entropy (PSE) with increasing wavelet packet decomposition levels for representative arc signals. It can be observed that during the initial decomposition layers, the PSE remains nearly constant at a high level, indicating that signal energy is broadly distributed in the frequency domain and that noise components are still dominant.

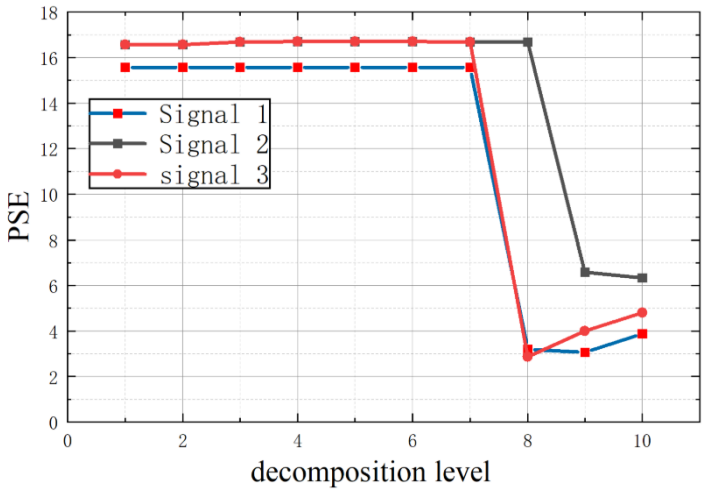

Fig.8. Variation of power spectral entropy (PSE) with wavelet packet decomposition level for representative arc signals.

When the decomposition level reaches approximately the 8th–9th layer, the PSE exhibits a sharp and abrupt decrease, accompanied by a significant increase in energy concentration. This cliff-like transition indicates an effective separation between noise and signal components, where high-frequency disturbances are strongly suppressed and the essential characteristics of the arc signal become prominent. Further decomposition beyond this point leads to a rise in PSE, suggesting over-decomposition and potential distortion of effective signal components.

This consistent jump behaviour observed across different arc signals provides a clear physical basis for determining the adaptive stopping criterion of wavelet packet decomposition.

The data show that the entropy values show three distinct phases corresponding to the three experimental days. On each day, the initial entropy values of the arc signals start relatively low, increase with repeated experiments, and eventually stabilise. This trend likely reflects

changes in the gas composition within the GIS chamber caused by repeated discharges, which alter the complexity of the arc signals. By the following day, the overnight resting period appears to have allowed the gas composition to recover, resulting in lower initial entropy values at the start of each new experimental day.

Despite the observed entropy variations, this study's primary objectives remain unaffected. The emphasis is on denoising the arc signals and precisely determining the ignition and extinction time points to provide critical positional information based on motor power signals. As a result, changes in entropy caused by gas composition changes within the GIS chamber do not warrant further investigation because they do not jeopardise the effectiveness of the proposed diagnostic approach.

Fig. 9 illustrates the distribution of power spectral entropy for arc signals before and after denoising over three consecutive days. The left-hand column represents the reconstructed power spectral entropy after denoising, while the right-hand column shows the initial power spectral entropy of the original signals.

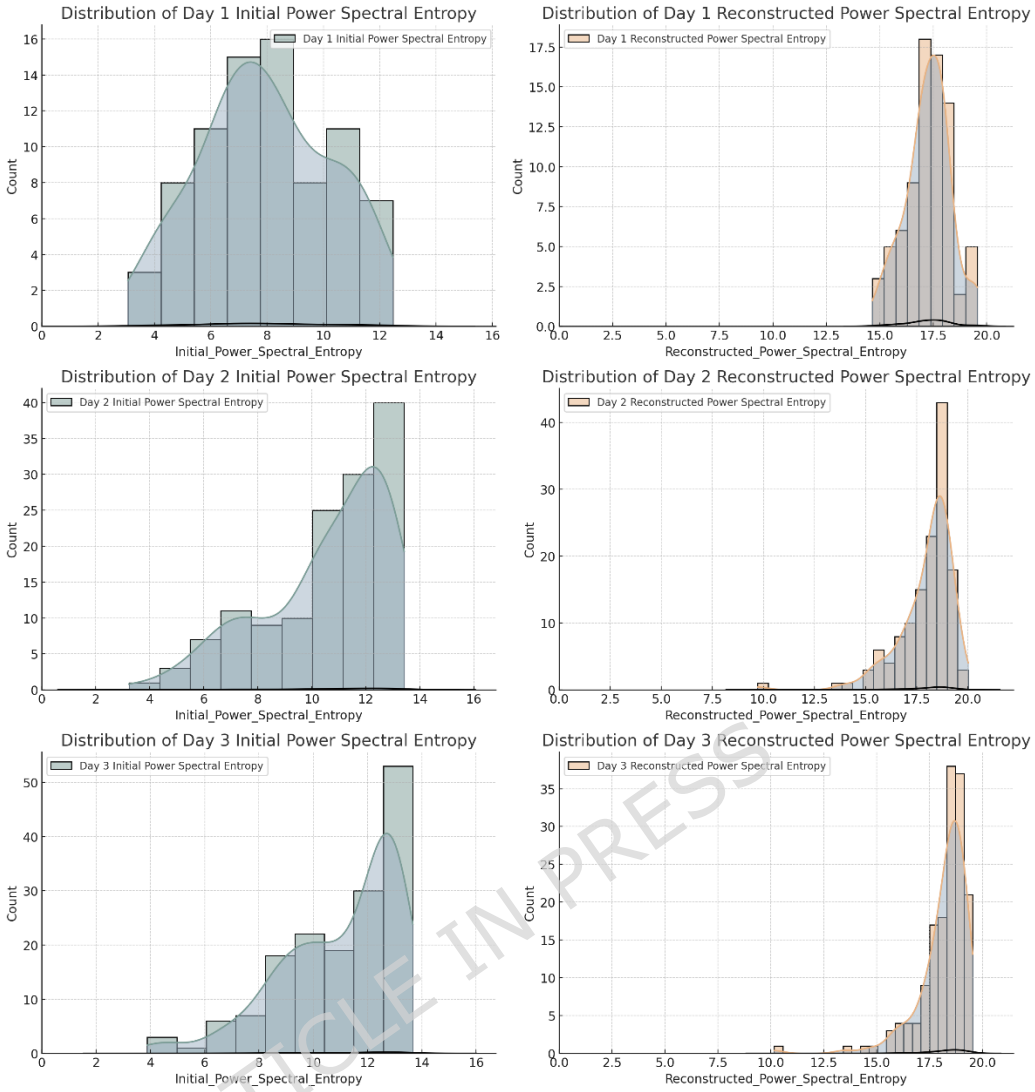

Fig. 9. Distribution of power spectral entropy.

The initial entropy distributions to the right show that the entropy values are relatively concentrated, indicating the presence of noise. Noise components add a uniform level of randomness to the signal, resulting in entropy values that fall within a narrow range. In contrast, arc signals are inherently complex, with each discharge having a distinct feature. This complexity is obscured by noise in the original signals, reducing variability in the entropy distribution.

After denoising, the reconstructed entropy values, as shown in the left column, are more evenly distributed. This broader distribution emphasises the removal of noise and the increased visibility of the arc signal's inherent variability. The denoising process effectively preserves each discharge event's distinct characteristics, revealing the arc signals' underlying structure in greater depth. This improvement ensures that critical features, such as ignition and extinction points, are easily identified for further investigation.

Once the arc signals have been successfully denoised, their increased clarity enables precise synchronisation with motor power signals. This synchronisation accurately identifies critical time points, such as the arc's ignition during contact separation and extinction during contact engagement. These time points correspond to specific phases of the motor power curve, providing valuable insights into the mechanical behaviour of the GIS disconnector.

Specifically, during the closing process, the disappearance of the arc indicates the onset of metal-to-metal contact, which can be cross-referenced with motor power data to evaluate whether sufficient overtravel has occurred. This procedure ensures proper contact engagement and minimises the risk of high contact resistance. On the other hand, during the opening process, the onset of the arc marks the beginning of contact separation. Synchronising this point with motor power analysis allows us to determine whether the separation distance meets safety standards.

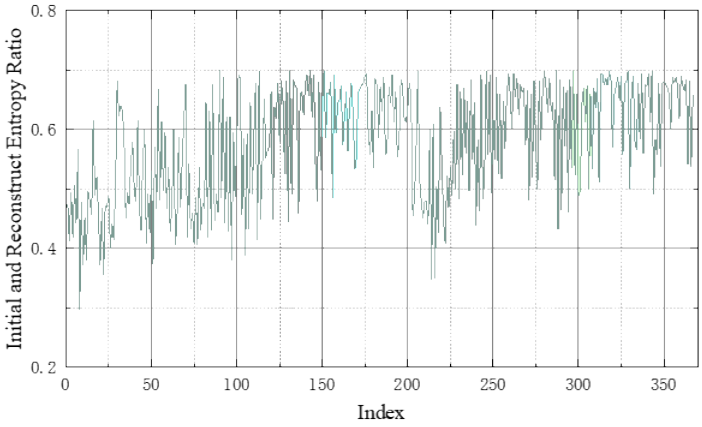

Fig. 10. Ratio of reconstruct and initial entropy.

The power spectral entropy before and after denoising generally ranged from 0.35 to 0.7 as shown in Fig. 10, with four data sets showing significant drift. Because the entropy value changes stepwise after each decomposition, a ratio of 0.65 was applied, and effective denoising was achieved for 365 of the 367 data sets. However, over-decomposition occurred for data sets with index numbers 56 and 105. Thus, the effectiveness was 99.46%. The two denoising-failed datasets were attributed to data acquisition constraints rather than algorithmic limitations, where several arc pulse peaks exceeded the oscilloscope recording range and were exported as null values, leading to signal discontinuity and denoising failure.

5.4. Validation on Different GIS Disconnectors

Data from a 220 kV three-phase split-type disconnector and another 110 kV GIS disconnector were collected under live switching conditions to validate the proposed method’s effectiveness and generalisability. Fig. 11 shows the experimental setups for these devices, while Fig. 12 shows the

recorded motor power and arc signals during their opening and closing operations.

(a) 220 kV GIS disconnector

(b) 110 kV GIS disconnector

Fig. 11. GIS disconnector with supplementary experimental data

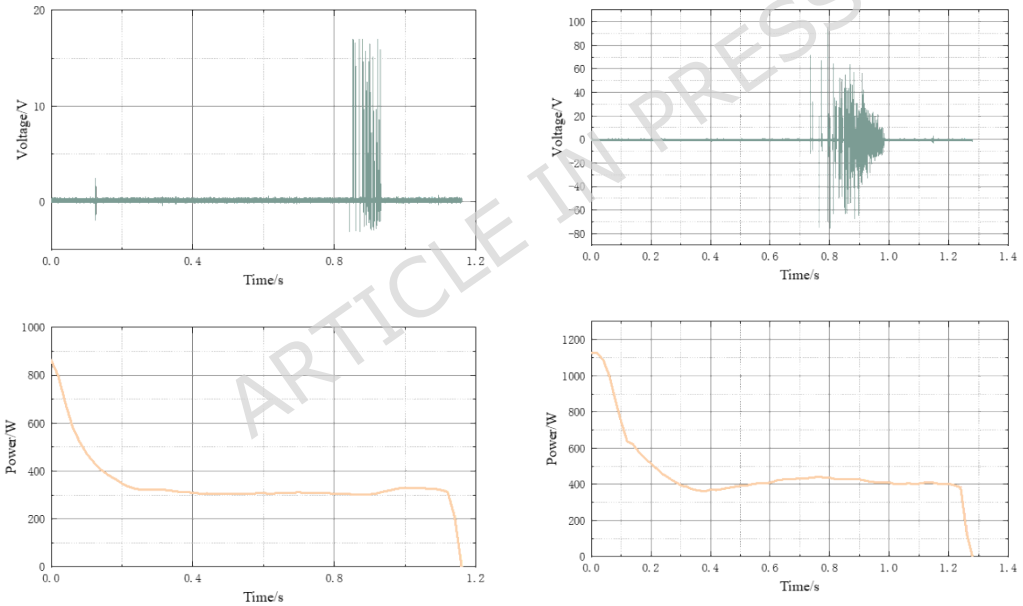

(a) The drive motor (bottom) and the corresponding discharge signal (top) during the closing process of a 220 kV GIS.

(b) The drive motor (bottom) and the corresponding discharge signal (top) during the closing process of a 110 kV GIS.

Fig. 12 The drive motor and the corresponding discharge signal during the closing process.

The results indicate that the arc signal characteristics obtained from these two GIS disconnectors are highly consistent with those observed in the initial experiments using the ZF12B-126 model, confirming the proposed method's applicability and reliability across different GIS disconnector types.

The discharge process occurs inside the sealed chamber of a GIS isolation switch, where humidity is relatively constant. Temperature can impact the discharge process. In addition, several other factors influence the discharge, including busbar voltage, the phase of the busbar voltage at the time of discharge, the speed of the moving contacts, internal gas pressure, and gas composition.

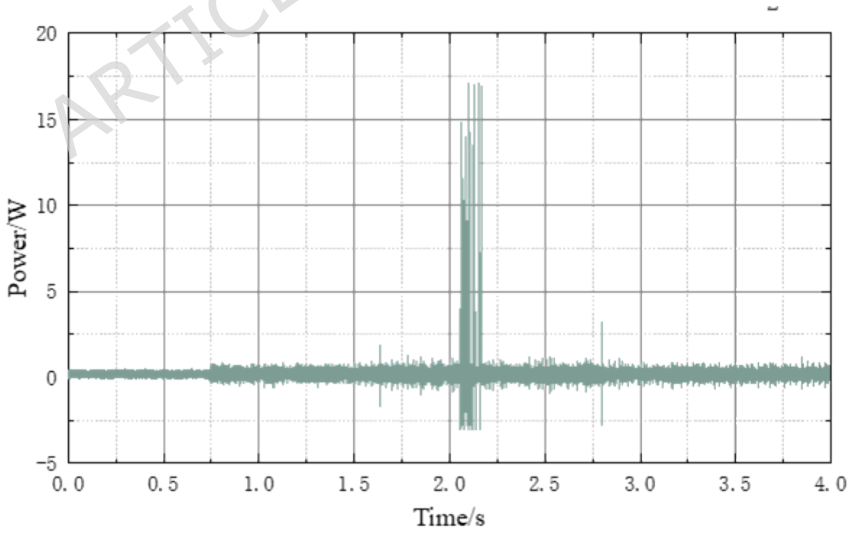

Fig. 13. Signal of a closing process of a 220 kV GIS disconnector.

Fig. 13 depicts the time-domain waveform of the Rogowski coil's induced voltage recorded during the closing process of a 220 kV GIS

disconnector, from busbar energisation to switching completion. The busbar is energised at around 0.75 s. Before this point, the signal appears as a relatively uniform, white noise-like waveform, primarily caused by the oscilloscope's internal power ripple. However, after busbar energisation, the waveform contains noise signals of varying amplitudes and envelope characteristics. The oscilloscope used in the experiment was powered by a separate mobile power supply, which effectively isolated potential noise coupling through the oscilloscope's ground wire after busbar energisation. The results show that the energised busbar causes additional acquisition noise. While this study does not look into the specific coupling mechanisms of this noise, its existence is demonstrated.

Additional experiments were conducted on arc signals collected from two different GIS disconnector models during their closing processes to further validate the effectiveness of the proposed denoising approach. Fig. 14 depicts the denoising results using the proposed method, which effectively reduces noise in different noise conditions, improving the clarity of the arc signal and demonstrating its robustness and applicability.

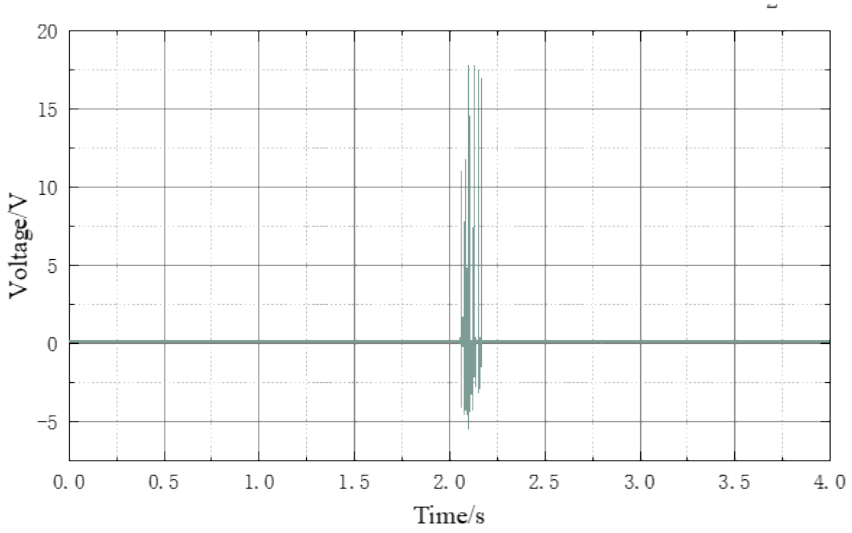

Fig. 14. Denoising results using the proposed method applied to another GIS signal.

This integrated approach, which combines arc signal analysis and motor power synchronisation, provides a robust diagnostic tool for identifying faults such as refusal to close or open, insufficient closing strokes, and inadequate opening distance. By capturing both arc characteristics and motor behaviours in real-time, this method improves the reliability of GIS disconnector diagnostics, reduces maintenance risks, and ensures system stability.

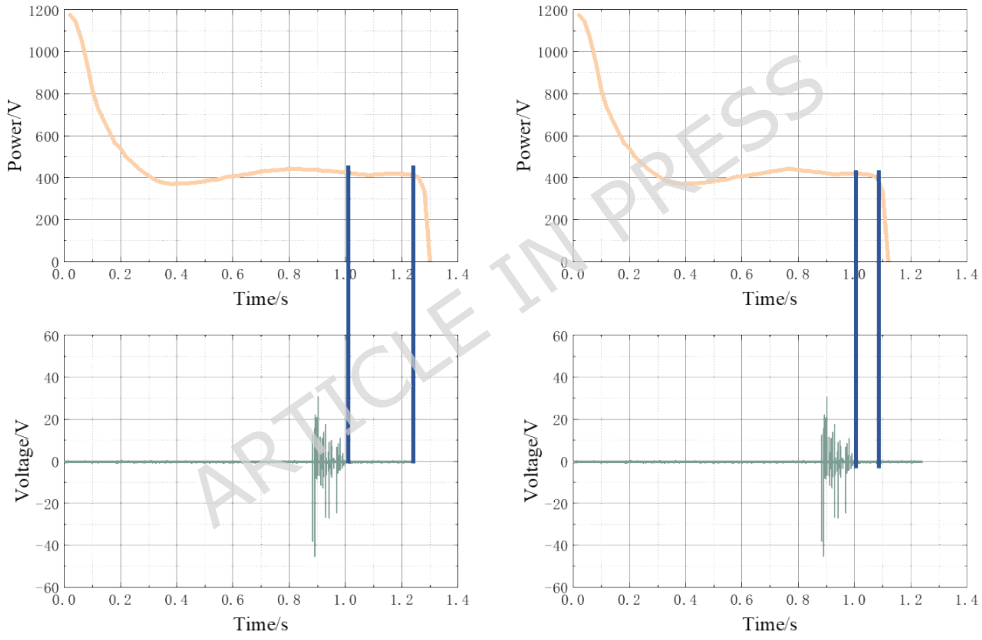

Fig.15. Comparison of synchronized arc signal and motor power under normal closing and insufficient overtravel conditions.

To further demonstrate the fault diagnosis capability of the proposed method, comparative experiments were conducted on the same experimental platform under both normal closing conditions and a simulated insufficient overtravel condition，Fig15. The closing operation

of the GIS disconnector was simulated by synchronously acquiring the arc signal and the motor power signal.

Under normal closing conditions, the time interval between the extinction of the arc signal and the end of the motor power signal was measured as 0.231 s, indicating sufficient overtravel after the initial contact. In contrast, under the simulated insufficient overtravel condition, the motor power signal terminated noticeably earlier, and the extinction of the arc signal occurred much closer to the motor power endpoint, resulting in a reduced overtravel time of 0.112 s.

This reduction in overtravel indicates that the disconnector failed to complete a proper closing operation. In such cases, insufficient contact area may lead to increased contact resistance and an unreliable electrical connection, thereby affecting normal current conduction. The comparative results demonstrate that the proposed method can effectively distinguish between normal operation and a representative mechanical fault scenario based on physically meaningful diagnostic parameters.

6. Conclusion

This study presents a novel diagnostic approach that combines arc signal detection and motor power analysis to address the challenges of mechanical fault diagnosis in GIS disconnectors. The mechanical condition of GIS disconnectors, particularly critical points such as initial separation and contact points, is critical to ensuring power system reliability. Traditional methods rely solely on motor power analysis and frequently fail to identify these points correctly due to a lack of distinguishing criteria.

This study incorporates arc signals—a previously underused diagnostic indicator—into the fault analysis framework to overcome these limitations. Arc signals generated during contact engagement and separation provide precise timing information about arc ignition and extinction. Synchronising these signals with motor power data allows for calculating key mechanical parameters such as overtravel distance, contact engagement, and separation distance, providing a comprehensive assessment of the GIS disconnector's operational state.

This study's key innovation is the adaptive wavelet packet decomposition technique guided by power spectral entropy. This method removes environmental and circuit-induced noise while preserving the arc signal's key features. The method achieves optimal denoising without unnecessary computational complexity by adaptively halting decomposition at an entropy-defined threshold. The enhanced signal clarity ensures the accurate identification of critical points, enabling precise fault diagnosis.

Experimental validation on a comprehensive testing platform confirms the proposed method's robustness and reliability. This platform accurately diagnoses key mechanical faults such as refusal to close or open, insufficient closing stroke, and inadequate opening distance. Additionally, entropy trend analysis across multiple test scenarios demonstrates the method's adaptability to changing signal conditions.

This study advances GIS disconnector diagnostics by combining the strengths of arc signal and motor power analysis. The proposed method improves fault detection precision while laying the groundwork for future

research into non-invasive diagnostic technologies for high-voltage equipment. Future research could concentrate on real-time implementation and broader adaptation for in-service monitoring, improving operational reliability and lowering maintenance costs.

Acknowledgments

Not applicable.

Author contribution

Song He: Conceptualization, Data curation, Formal analysis, Methodology, Validation, Visualization, Writing - original draft**. Jiangjun Ruan:** Supervision**. Yufei Liu:** Validation. **Feiyue Yan:** Validation. **Rui Luo:** Validation.

Data Availability

The datasets generated during and/or analysed during the current study are available from the corresponding author on reasonable request.

Competing Interests Statement

The author(s) declare no competing interests.

Funding

No funds, grants, or other support was received.

Ethics declarations

The authors have nothing to report.

Consent to participate/Consent to publish

Not applicable.

References

[1] Zhang, Z. et al. Gas-insulated switch-gear mechanical fault detection based on acoustic using feature fused neural network. *Electr. Pow. Syst. Res.* **230**, 110226 (2024). https://doi.org/10.1016/j.epsr.2024.110226.

[2] Lin, L., Wang, B., Qi, J., Chen, L. & Huang, N. A novel mechanical fault feature selection and diagnosis approach for high-voltage circuit breakers using features extracted without signal processing. *Sensors.* **19**, 288 (2019). https://doi.org/10.3390/s19020288.

[3] Yu, G., Xie, M., Liang, J., Farooq, A. & Williams, E.J. A GIS-based 3D slope stability analysis method based on the assumed normal stress on the slip surface. *Sci Rep.* **10**, 4442 (2020). https://doi.org/10.1038/s41598-020-61301-x.

[4] Abbasi, A.R. Fault detection and diagnosis in power transformers: a comprehensive review and classification of publications and methods. *Electr. Pow. Syst. Res.* **209**, 107990 (2022) . https://doi.org/10.1016/j.epsr.2022.107990.

[5] He, R., Yan, J., Zhao, D., Lu, L. & Geng, Y. Gas-insulated switchgear partial discharge acoustic–electric joint localisation method based on the salp swarm algorithm and least squares estimation. *Measurement.* **225**, 114020 (2024). https://doi.org/10.1016/j.measurement.2023.114020.

[6] Qiu, Z., Ruan, J., Huang, D. & Huang, Y. Mechanical fault diagnosis of high voltage outdoor disconnector based on motor current signal analysis, in 2014 International Conference on Power System Technology, Chengdu, China, (2014). https://doi.org/10.1109/POWERCON.2014.6993501.

[7] Tao, P., Chaohui, L., Yi, D., Feng, L. & Sheng, D. Mechanical Fault Diagnosis of High Voltage Disconnector Based on Motor Current Detection, in 2019 IEEE 3rd Information Technology. Networking, Electronic and Automation Control Conference (ITNEC), Chengdu, China. (2019). https://doi.org/10.1109/ITNEC.2019.8729509.

[8] Zhong, Y., Gong, R.L., Su, S., Hao, J., Wang, Q., Jiang, X.: Identification Method of Abnormal Contact Defect on GIS Conductor Base and Disconnector Contact Based on Ensemble Empirical Mode Decomposition, in 2020 8th International Conference on Condition Monitoring and Diagnosis (CMD), Phuket, Thailand. (2020). https://doi.org/10.1109/CMD48350.2020.9287282.

[9] Jia, Y. et al. Research of the vibration characteristics in GIS Disconnector under different Contact State, in 2018 IEEE International Conference on High Voltage Engineering and Application (ICHVE), Athens, Greece. (2018). https://doi.org/10.1109/ICHVE.2018.8641928.

[10] Ding, Y., Zhong, Y., Wang, X., Hao, J. & Jiang, X. Difference and Analysis of Mechanical Vibration Signal Characteristics between Mechanical Defects and Partial Discharge Defects of Gas Insulated Switchgear, in 2021 IEEE 5th International Conference on Condition

Assessment Techniques in Electrical Systems (CATCON), Kozhikode, India. (2021). https://doi.org/10.1109/CATCON52335.2021.9670536.

[11] Lin, S., Zhang, K. & Wang, Q. Fault Diagnosis Method of Disconnector Based on Operating Torque in Closing Process, in 2021 IEEE 2nd China International Youth Conference on Electrical Engineering (CIYCEE), Chengdu, China. (2021). https://doi.org/10.1109/CIYCEE53554.2021.9676840.

[12] Zhou, T., Ruan, J., Liu, Y., Peng, S. & Wang, B. Defect Diagnosis of Disconnector Based on Wireless Communication and Support Vector Machine. *IEEE Access.* **8**, 30198-30209 (2020). https://doi.org/10.1109/ACCESS.2020.2972010.

[13] Yuan, Y. et al. Fault Diagnosis in Gas Insulated Switchgear Based on Genetic Algorithm and Density- Based Spatial Clustering of Applications With Noise. *IEEE Sens. J.* **21**, 965-973 (2019). https://doi.org/10.1109/JSEN.2019.2942618.

[14] Wang, Q., Zhang, K. & Lin, S. Fault Diagnosis Method of Disconnector Based on CNN and D-S Evidence Theory. *IEEE T. Ind. Appl.* **59**, 5691-5704 (2023). https://doi.org/10.1109/TIA.2023.3284780.

[15] Wang, X. Fault arc Identification Method of PV System Based on Subband Energy after Wavelet Packet Decomposition, in 2022 7th International Conference on Power and Renewable Energy (ICPRE), Shanghai, China. (2022). https://doi.org/10.1109/ICPRE55555.2022.9960329.

[16] Zhang, S., Zhou, K. & Zhang, D. "Study on Identification of Off-line Arcing Based on Wavelet Packet Decomposition and Neural Network," 2020 6th Global Electromagnetic Compatibility Conference (GEMCCON), XI'AN, China, pp.1-4, (2020). doi: 10.1109/GEMCCON50979.2020.9456673.

[17] Zhou, F. et al. Identification for Abnormal Electrical Phenomenon in Vehicle-grid Coupling System Based on Wavelet Packet Decomposition and Neural Network, in 2021 IEEE Sustainable Power and Energy Conference (iSPEC), Nanjing, China. (2021). https://doi.org/10.1109/iSPEC53008.2021.9735996.

[18] Vulpe, A., Zamfirache, M. & Caranica, A. Analysis of Spectral Entropy and Maximum Power of EEG as Authentication Mechanisms, in 2023 International Conference on Speech Technology and Human-Computer Dialogue (SpeD), Bucharest, Romania. (2023). https://doi.org/10.1109/SpeD59241.2023.10314890.

[19] Rusnac, A.L. & Grigore, Q. Intelligent Seizure Prediction System Based on Spectral Entropy, in 2019 International Symposium on Signals, Circuits and Systems (ISSCS), Iasi, Romania. (2019). https://doi.org/10.1109/ISSCS.2019.880179.